Photon correlation spectroscopy of polydisperse systems

J. Briggs and D. F. Nicoli

Citation: The Journal of Chemical Physics **72**, 6024 (1980); doi: 10.1063/1.439057
View online: http://dx.doi.org/10.1063/1.439057
View Table of Contents: http://scitation.aip.org/content/aip/journal/jcp/72/11?ver=pdfcov
Published by the AIP Publishing

Photon correlation spectroscopy of polydisperse systems[a)]

J. Briggs[b)] and D. F. Nicoli

Department of Physics, University of California, Santa Barbara, Santa Barbara, California 93106
(Received 31 October 1979; accepted 8 January 1980)

Using the method of cumulants, we investigate the distribution of diffusion coefficients in polydisperse systems. We consider the intensity weighting for distributions of spherical particles having the same polarizability. Results of computer simulations are presented for a variety of polydisperse situations. Also, comparisons are made between predicted and measure results for mixtures of Dow latex spheres.

I. INTRODUCTION

Photon correlation spectroscopy has proven to be a valuable method for investigating the properties of disperse systems of submicron particles. Chu,[1] Cummins and Pike,[2,3] and Berne and Pecora[4] review the field and provide excellent bibliographies. Contrary to the real situation, one usually assumes scattering from a monodisperse sample. The effects of polydispersity have been considered by several authors.[5–11] Some of these treatments[5,6] are restricted to Schulz distributions of rods and coils. Others[5–10] are restricted to unimodal distributions of finite width or to bimodal distributions, each of infinitesimal width. Still others[10,11] allow the intensity weighting associated with a particle type to be an adjustable parameter. One of these[8] compares the theoretical predictions for the mean diffusion coefficient in the case of bimodal mixtures of latex spheres, with values measured with a spectrum analyzer. We expand upon this earlier work in the following ways: our theory accounts for the finite width of each modal, we use a 4-bit, 10 MHz autocorrelator to make the measurements, and we compare measured and theoretical values of both the mean and standard deviation of the distribution of diffusion coefficients.

The purpose of this paper is to give a general view of the effects of polydispersity on dynamic light scattering measurements. In Sec. II we give the most general intensity weighting that accompanies each component of the time correlation function of the scattered E field from a polydisperse system. The inclusion of particle form factors guarantees that intraparticle interference is allowed. The analysis is then restricted to spherical particles, with the same uniform polarizability. The method of cumulants, due to Koppel,[10] is used to relate the parameters of the distribution of translational diffusion coefficients to the intensity weighted distribution of radii. We consider the mean, variation (standard deviation relative to the mean), and skewness. These parameters were calculated by computer simulation, where the particle radius distribution was characterized by one or two Gaussians of variable mean, standard deviation, and relative height (in the bimodal cases). Results are given in Sec. III. In addition to unimodal systems, we consider bimodal systems where the components have the same variation, but the mean of the secondary component is 50% or 100% larger than the mean of the primary. We vary the primary mean and the relative number of the secondary, to model the effects of polydispersity by aggregation. In a second type of bimodal system we model the more contrived situation in which all samples are contaminated by a very small number of particles from a broad secondary distribution.

In Sec. IV predicted and measured values for mixtures of Dow latex spheres (0.091 and 0.234 μ diameters) are compared. We examine the radius associated with the mean diffusion coefficient and the variation in the distribution of diffusion coefficients as the proportion of the larger sphere among the smaller varies between 10^{-4} and 10^{-1} (number concentration). The predicted and measured radii compare well and the trend of the predicted variation is clearly revealed in the measured results.

II. LIGHT SCATTERING FROM A POLYDISPERSE SYSTEM OF PARTICLES

The temporal and spectral characteristics of the scattered irradiance from monodisperse systems in both homodyne and heterodyne experimental configurations have been extensively treated in the literature.[1–4] The present discussion will be limited to polydisperse systems within the context of a homodyne experiment where the time correlation of the scattered irradiance is measured. It is well known[12] that when Gaussian statistics are obeyed, the time correlation of the scattered irradiance may be reduced to produce the following function,

$$C(\tau) = \tfrac{1}{2}\ln[\langle I(t)\,I(t+\tau)\rangle - \langle I\rangle^2] \tag{1}$$

$$= \ln[\langle I\rangle\,|g^{(1)}(\tau)|\,], \tag{2}$$

where

$$g^{(1)}(\tau) = \frac{\langle E(t)E^*(t+\tau)\rangle}{\langle I\rangle}\ , \tag{3}$$

$$|g^{(1)}(\tau)| = \exp(-DK^2\tau)\ . \tag{4}$$

The right-hand side of Eq. (1) is measurable to within an additive constant, where the baseline $\langle I\rangle^2$ may be either directly measured or calculated from the average counting rate. Equation (4) assumes that the system is monodisperse, in which case by Eq. (2), $C(\tau)$ will be linear with a slope proportional to DK^2, where D is the translational diffusion coefficient and K is the scattering wave number.

[a)]This work was partially supported by the UCSB Research Committee and by a research grant from Colby College.
[b)]On leave from the Department of Physics, Colby College, Waterville, ME 94901.

 0021-9606/80/116024-07$01.00

In our model for a polydisperse system, members of a particle type will have the same size, shape, and polarizability. Then, the E fields in Eq. (3) become summations over particle types. The field scattered by a j-type particle is proportional to the particle volume v_j, a polarizability factor β_j (that accounts for the fluctuation of its polarizability from the volume-average polarizability and local-field effects[13]), and the particle form factor G_j. That is, the scattered E field from the N_j, j-type particles is

$$E_j \propto v_j \beta_j G_j \sum_{i=1}^{N_j} \exp(i\mathbf{K}\cdot\mathbf{r}_i) , \tag{5}$$

where $\mathbf{K}$ is the scattering wave vector and $\mathbf{r}_i$ gives the position of the ith, j-type particle. The statistical nature of the random-walk summation (for disperse systems) in Eq. (5) is that

$$\langle I_j \rangle \propto N_j (v_j \beta_j G_j)^2 . \tag{6}$$

Using Eqs. (3), (4), and (6), and the fact that different type particles are statistically independent, we may write an expression for the intensity-weighted magnitude of the first-order correlation function,

$$\langle I \rangle |g^{(1)}(\tau)| = (\text{const}) \sum_j N_j (v_j \beta_j G_j)^2 \times \exp(-D_j K^2 \tau) . \tag{7}$$

Equation (7) gives the appropriate intensity weighting within combinations of translational diffusional processes that cause the relaxation of scattered intensity fluctuations from polydisperse systems. It allows particle types to be distinguished by size, shape, and polarizability.

We shall now restrict ourselves to systems of spheres, all of the same uniform polarizability. Then, the only variables are the relative numbers and radii of particle types. Accordingly, we shall rewrite Eq. (7), retaining only the dependencies on these variables.

$$\langle I \rangle |g^{(1)}(\tau)| = (\text{const}) \left(\frac{\sum_j I_j \exp(-\rho/R_j)}{\sum_j I_j} \right) \equiv (\text{const}) \langle \exp(-\rho/R_j) \rangle_{I_j} , \tag{8}$$

where

$$I_j \equiv N_j R_j^6 G_j^2 . \tag{9}$$

We have assumed infinite dilution to write

$$D_j K^2 \tau = \frac{kT}{6\pi\eta R_j} K^2 \tau \equiv \rho/R_j ,$$

where k is the Boltzmann constant, T is the temperature, and η is the solvent viscosity. The form factor of a spherical particle is

$$G_j = 3 \left(\frac{\sin(Z_j) - Z_j \cos(Z_j)}{Z_j^3} \right) ,$$

where

$$Z_j \equiv K R_j = 4\pi n (R_j/\lambda) \sin|\theta/2| .$$

We shall use the method of cumulants, as reviewed by Koppel,[10] to reduce the function $C(\tau)$, Eq. (1), which may be derived from the measured time correlation of the scattered irradiance. Combining Eqs. (2) and (8), we write

$$C(\tau) = \ln[\langle \exp(-\rho/R_j) \rangle_{I_j}] + (\text{const}) ,$$

which in terms of cumulants reduces to

$$C(\tau) = \sum_{m=0}^{\infty} \frac{(-\rho)^m}{m!} \mathcal{K}_m . \tag{10}$$

In Eq. (10), $\mathcal{K}_m$ is the mth cumulant, for example $\mathcal{K}_1 = \mu_1$, where μ_m is the intensity-weighted mth moment of the *inverse* of the radius,

$$\mu_m = \langle R_j^{-m} \rangle_{I_j} . \tag{11}$$

In this fashion the cumulants characterize the distribution of diffusion coefficients (henceforth referred to as the D distribution) that contribute to the relaxation of scattered irradiance fluctuations. Consider the unimodal system where the particle radius distribution (henceforth, the R distribution) is a Gaussian. The D distribution will be non-Gaussian owing to the intensity weighting and to the fact that the translational diffusion coefficient is proportional to the inverse of the radius. Hence, the radius associated with the mean diffusion coefficient will not equal the mean of the R distribution. Also, the D distribution will be skewed even for the case of a Gaussian R distribution.

In principle, given the relative number and radius of each particle type, the cumulants may be determined. The problem in analyzing experimental results is to do the *reverse*. After measuring $C(\tau)$, a low order polynomial (typically quadratic or cubic) is least-squares fitted to the data to determine the first few cumulants. The question is, given these first few cumulants with their experimental uncertainty, what can we say about the R distribution. To deal with this question we performed a computer simulation that accepts an R distribution, in terms of one or more Gaussians, and then calculates the first three cumulants. The results are presented in the next section.

III. SIMULATION OF POLYDISPERSE SYSTEMS

In the simulation, particles are classified by species. Each species is characterized by a relative number density and the mean and standard deviation of a Gaussian R distribution. A system will be designated unimodal, bimodal, etc., according to the number of species. The results presented in this section will refer to the following parameters:

N_i	Relative number density, ith species
$\bar{R}_i$	Mean radius, ith species
$Z_i = K\bar{R}_i = \frac{4\pi n \bar{R}_i}{\lambda} \sin\|\theta/2\|$	Dimensionless mean, ith species
V_{R_i}	Variation, ith species
$\bar{R}_{\text{tot}}$	System mean radius

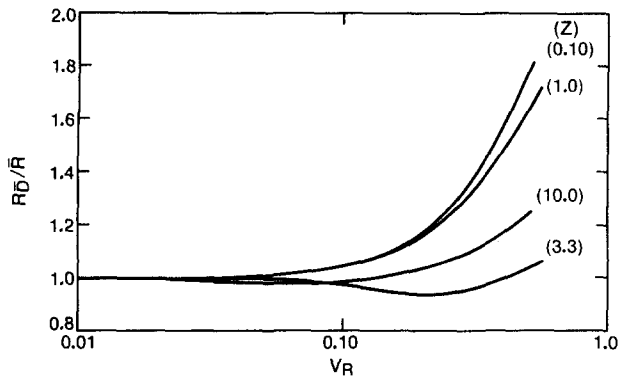

FIG. 1. For unimodal systems, $R_{\bar{D}}/\bar{R}_{tot}$ versus V_R for various Z [$Z = KR = 4\pi n(R/\lambda)\sin|\theta/2|$].

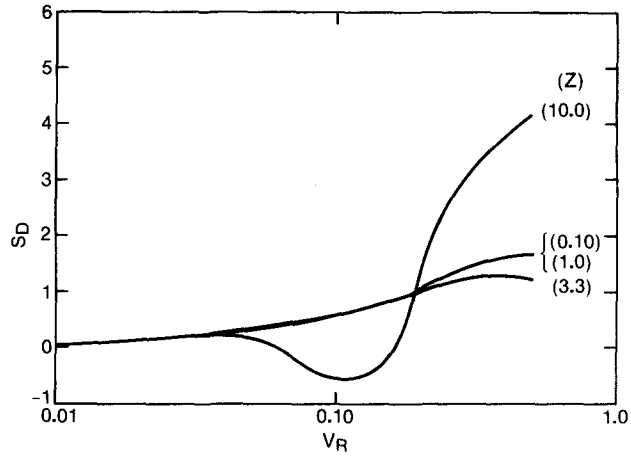

FIG. 3. For unimodal systems, S_D versus V_R for various Z.

$R_{\bar{D}} = \mathcal{K}_1^{-1}$	Radius of spherical particle with the system mean diffusion coefficient
$V_D = \mathcal{K}_2^{1/2}/\mathcal{K}_1$	Variation of the D distribution
$S_D = \mathcal{K}_3/\mathcal{K}_2^{3/2}$	Skewness of the D distribution.

Recall that the variation of a Gaussian distribution is the standard deviation relative to the mean (normalized standard deviation). In the calculation of the intensity-weighted moments, Eq. (11), the dimensionless parameter Z is significant. We shall give results for values of Z between 0.1 and 10. To relate this to a physical situation, if the solvent is water (index of refraction equal to 1.33) and the wavelength is 514.5 nm (green argon line) with a scattering angle of 90°, then the case $Z=1$ corresponds to a particle radius of 435 Å. Integrations were performed on a PDP-11/34 computer by dividing the Gaussian of each species into 72 intervals extending over ±6 standard deviations, and summing. (When this range extended to negative radii, only the intervals corresponding to positive radii were included.) The accuracy of this integration routine is such that the uncertainties in the calculated parameters of the D distribution, through the third order, are always less than 0.1%

First, consider unimodal systems. Figure 1 plots $R_{\bar{D}}/\bar{R}_{tot}$ versus V_R for various Z. Bargeron[8] gives

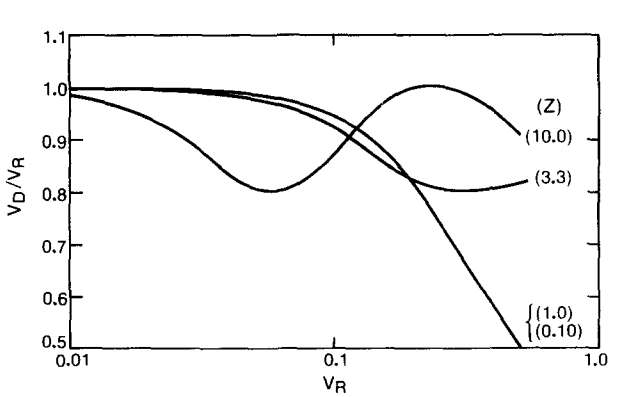

FIG. 2. For unimodal systems, V_D/V_R versus V_R for various Z.

similar results which are based on an approximate analytical approach and are thus restricted to the following regimes: $Z \ll 1$ and $V_R \lesssim 0.25$ *or* $Z \lesssim 1$ and $V_R \lesssim 0.1$. From Fig. 1 we see that for $Z \lesssim 1$, the response is dominated by the intensity weighting that goes like R^6 for small particles. Thus, as the R distribution broadens, $R_{\bar{D}}/\bar{R}_{tot}$ rapidly increases. For $Z > 1$, the intraparticle interference causes certain radii to be more or less significant than others. Now as V_R increases, the successive inclusion of such particles causes structure in the response of $R_{\bar{D}}/\bar{R}_{tot}$. We note that these interference effects may result in $R_{\bar{D}}/\bar{R}_{tot}$ less than unity. This is because the intensity weighting function, Eq. (9), decreases with increasing R just before zeros in the form factor G. Hence, when the R distribution samples such a region (e.g., $Z = 3.3$ and $V_R = 0.2$), the *smaller* radii of the distribution will dominate, causing $R_{\bar{D}}/\bar{R}_{tot} < 1$. Finally, note that the general rise in $R_{\bar{D}}/\bar{R}_{tot}$ is less pronounced for larger Z. This is because the intensity weighting goes from scaling like R^6 to increasing like R^2 as Z increases.

Figure 2 plots V_D/V_R versus V_R for the same set of Z. Again, Bargeron[8] gives similar results with the above mentioned limitations. In Fig. 2 we see V_D/V_R smoothly decreasing with increasing V_R for $Z \leq 1$. This is again due to the small particle intensity weighting which selects the larger particles of a distribution, resulting in a narrower effective D distribution. Intraparticle interference causes a more complicated behavior for $Z > 1$. Furthermore, the falloff in V_D due to intensity weighting is less pronounced in systems with $Z > 1$, again because the intensity weighting is less sharply rising with increasing radius. Figure 3 plots the skewness of the distribution of diffusion coefficients versus the variation in the radius. For $Z \leq 1$, S_D smoothly increases with V_R, again due to the intensity weighting that serves to skew, while sharpening, the distribution. For $Z > 1$, interference effects cause the skewness to oscillate about the small size behavior.

Next consider bimodal systems that mimic aggregation. Our naive model for aggregation assumes that the secondary species will possess radii which are either 50% or 100% larger than the primary distribution radii.

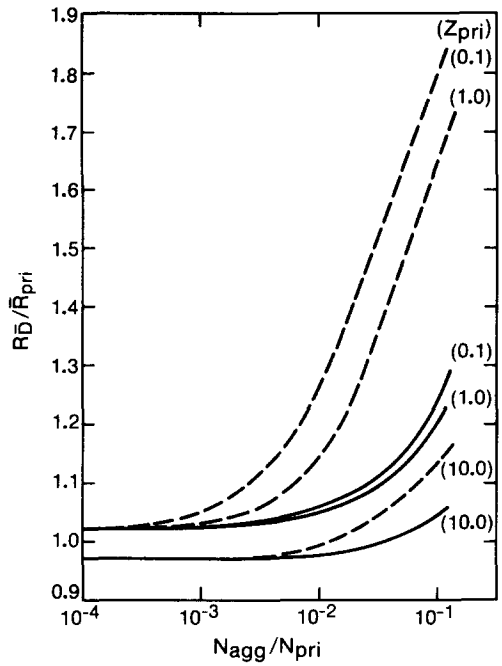

FIG. 4. For bimodal systems mimicing aggregation, $R_{\bar{D}}/\bar{R}_{pri}$ versus N_{agg}/N_{pri} for various Z_{pri}, where the aggregates are 50% (solid lines) and 100% (dashed lines) larger than the primary particles.

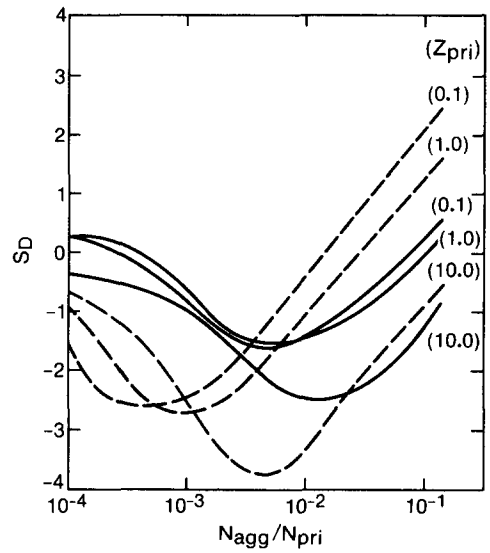

FIG. 6. For bimodal systems mimicing aggregation, S_D versus N_{agg}/N_{pri} for various Z_{pri}, where the aggregates are 50% (solid lines) and 100% (dashed lines) larger than the primary particles.

This assumes that the aggregates are formed from the primary particles with uniform probability as regards radius. Results will be presented for Z_{pri} equal to 0.1, 1, and 10 (recall our previous numerical example). Figures 4–6 give $R_{\bar{D}}/\bar{R}_{pri}$, V_D and S_D, respectively, versus the relative number aggregates per primary particle, N_{agg}/N_{pri}. In the case presented, the variation of both primary and secondary particle distributions is equal to 0.064. This was chosen because it corresponds to the variation which Dow Chemical Co. quotes for its 0.091 μ latex spheres. (Smaller variations are claimed for some of the larger spheres.)

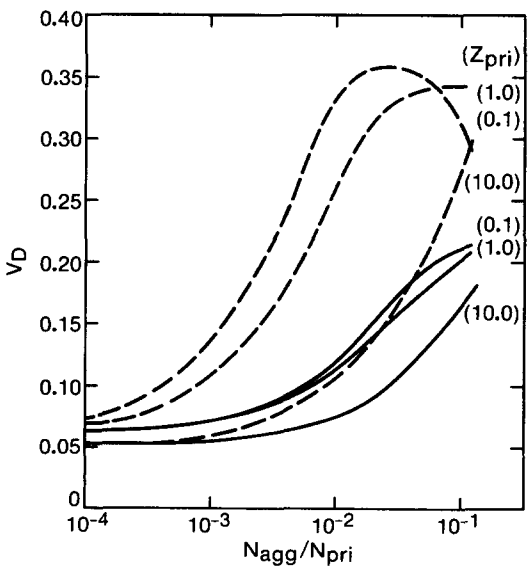

FIG. 5. For bimodal systems mimicing aggregation, V_D versus N_{agg}/N_{pri} for various Z_{pri}, where the aggregates are 50% (solid lines) and 100% (dashed lines) larger than the primary particles.

In Fig. 4 we see that polydispersity due to aggregation may have a significant effect on the size determined by the average diffusion coefficient. For example, the presence of one aggregate of twice the radius in a hundred particles with radii such that $Z=0.1$ results in a 26% error. Because the intensity weighting is less severe for larger particles, the error is smaller for larger Z; and, of course, the error is smaller for smaller aggregates. Figure 5 shows how aggregation results in variations in the D distribution larger than that of the radii. A 1% concentration of 100% larger aggregates for primary particles of $Z=0.1$ produces a V_D equal to about 0.29. The behavior with respect to primary particle size and the relative size of the aggregates is again as expected. The nature of the skewness S_D is certainly not intuitive. Because the skewness involves higher order moments than the variation and the mean, it is more sensitive to changes in the system parameters. Figure 6 presents S_D in the simulated system. The skewness for single species systems generally increases from zero with increasing variation in the radii, Fig. 3. Here, we see that for the small relative numbers of aggregates that we considered, the skewness starts out negative and becomes positive with further aggregation as the intensity weighting favors the larger particles.

Finally, we consider bimodal systems where the second component is not derived from the first. For the sake of illustration, we select a situation where the sample is contaminated by a small number of particles selected from a very broad R distribution. We shall take this distribution to have a mean of 0.5 μ and a variation of 0.4. (That is, these particles have radii ranging from zero up to a few microns.) We then consider primary particle distributions with means that

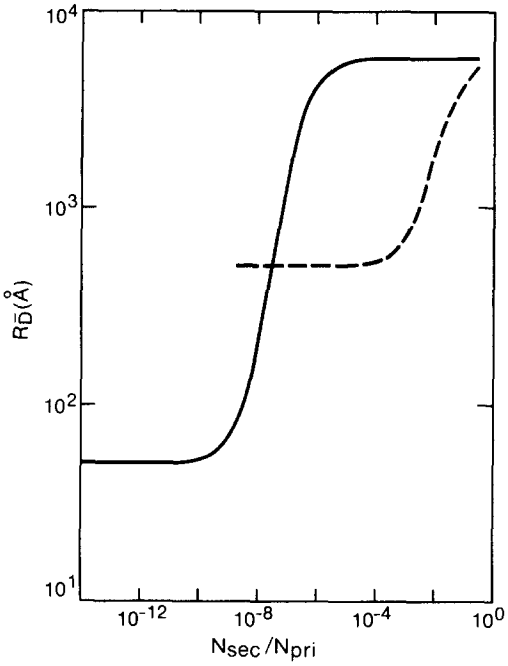

FIG. 7. For bimodal systems with a broad secondary R distribution ($\bar{R}_{sec} = 0.5$ μm, $V_{sec} = 0.4$), $R_{\bar{D}}$ versus N_{sec}/N_{pri}, for primary particles of radii equal to 50 (solid line) and 500 Å (dashed line).

are 100 and 10 times smaller than the mean of the above secondary R distribution; i.e., primary means of 50 and 500 Å. In both cases the primary particles are given variations equal to 0.064, like the Dow spheres. We now ask the question, as we increase the relative number of secondary particles, how does the D distribution change from that characteristic of the primary particles alone. Figure 7 plots $R_{\bar{D}}$ versus N_{sec}/N_{pri} for the two primary sizes. Note the very low relative number of secondary particles that cause a significant increase in $R_{\bar{D}}$ over $\bar{R}_{pri}$. Of course, small number ratios transcribe to considerably larger ratios of secondary particle weight to primary particle weight in some unit volume. Figure 8 plots V_D versus N_{sec}/N_{pri}. Note that the peak value of V_D is greater than the large variation assumed for the secondary particles. Also, at the low end, V_D starts to rise above $V_{R_{pri}}$ well before $R_{\bar{D}}$ has started to rise above $\bar{R}_{pri}$.

IV. MEASUREMENTS FROM POLYDISPERSE SYSTEMS

To test the validity of our ideas about polydispersity, we made measurements on mixtures of Dow latex spheres in water. We used spheres of diameter 0.091 and 0.234 μ. Each sample had 2.4×10^{10} particles/cc, but the ratio of the number of large spheres to small spheres per unit volume was varied between 10^{-4} and 10^{-1}. Scattered light from the 514.5 nm argon laser line was collected at an angle of 90°. We used a Nicomp Instruments Model 6864 Computing Autocorrelator (4-bit, 64 channel, 10 MHz) to collect data and perform the cumulants analysis. The autocorrelator makes least-squares fits to both second- and third-order polynomials using a built-in microcomputer. In each case, the baseline value may be either directly measured using a 1024-channel delay or calculated from bookkeeping channels. (The values obtained by these two procedures were essentially the same, thereby serving as a check on quality of the correlation function.)

Separate measurements were made with different input pulse rates and channel time widths. The following parameters were recorded: average counts per channel width (always $\lesssim 2$), relative correlation efficiency, and the number of exponential decays from first to last channel (ranging from 1.2 to 2.0). Measurements were discarded only if there was some discrepancy in one of these parameters. The correlation time was always such that there was a significant number of counts in the last channel relative to the baseline. The results presented here represent the averages of between 28 and 52 separately measured values for the various sample mixtures.

Figure 9 gives the measured values for $R_{\bar{D}}$ versus $N_{0.234}/N_{0.091}$ with the accompanying uncertainty ranges. The lateral uncertainty is due to the estimated mixing errors; the vertical uncertainty represents ±1 standard deviation of the measured average. The solid line plot is the $R_{\bar{D}}$ predicted by our simulation, where Dow's values for the radius and standard deviations were used. We note the excellent agreement between the predicted and measured mean values.

Figure 10 makes the corresponding comparison for V_D versus $N_{0.234}/N_{0.091}$. We know that V_D, being a second-order parameter, is even more significantly affected by sample contamination and uncertainty in the analytical procedure. Nevertheless, the trend of the predicted values for V_D is revealed in the measure-

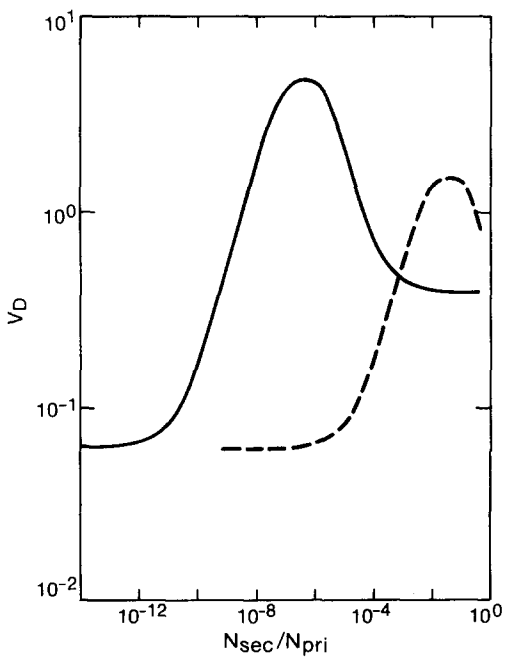

FIG. 8. For bimodal systems with a broad secondary R distribution ($\bar{R}_{sec} = 0.5$ μm, $V_{sec} = 0.4$), V_D versus N_{sec}/N_{pri}, for primary particles of radii equal to 50 (solid line) and 500 Å (dashed line).

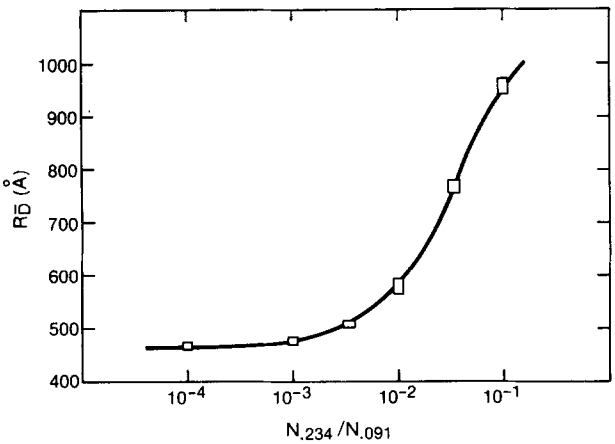

FIG. 9. Measured (boxes) and predicted (solid line) values of $R_{\bar{D}}$ versus $N_{0.234}/N_{0.091}$ for mixtures of Dow latex spheres (0.091 μm and 0.234 μm diameters).

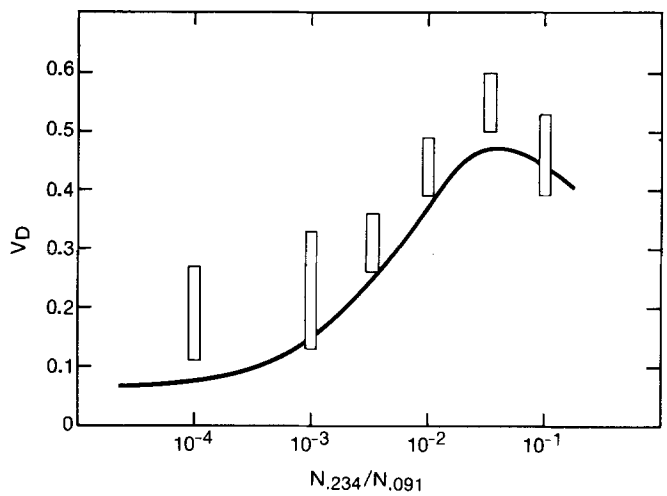

FIG. 10. Measured (boxes) and predicted (solid line) values of V_D versus $N_{0.234}/N_{0.091}$ for mixtures of Dow latex spheres (0.091 μm and 0.234 μm diameters).

ments. Possible explanations for the apparent offset of V_D^{exptl} above V_D^{theor} are: aggregation or an unknown second component in the sample; inaccurate standard deviations quoted by Dow; intrinsic error in baseline determination (e.g., laser noise contribution); a spurious heterodyne signal; and the finite range in the actual scattering angle. With regard to aggregation, we performed four component simulations in which each of the Dow species was allowed to aggregate. The aggregated radii were 100% larger. A good fit of V_D^{exptl} to V_D^{theor} was obtained for a 0.5% level of aggregation for each of the two species. Unfortunately, this alters $R_{\bar{D}}$ enough so that the quality of fit to the measured values is significantly compromised. Hence, we conclude that aggregation may cause a portion of the offset in Fig. 10, but not all of it. The other possible contributing factors need further investigation.

V. CONCLUSION

Working from first principles, we have dealt with the intensity weighting within a continuous distribution of particles, each portion of which contributes differently to the temporal characteristics of irradiance fluctuations. Through cumulants we have expressed the characteristics of the distribution of diffusion coefficients in terms of the intensity-weighted distribution of particles. In this fashion we have related the measurable parameters of a dynamic light scattering experiment to the physical characteristics of the polydisperse system. Our simulation procedure has established a straightforward technique of relating theoretical predictions to experimental results for any particle distribution. We have successfully applied this method for the case of mixtures of uniform spheres. Also, by giving the simulated results for a variety of polydisperse systems, we have provided a general view of the effects of polydispersity.

One might be concerned that the simulation does not account for factors which may affect the results of experiments. First, there are statistical errors due to the finite counting times. (The simulation has its own statistical errors which we have noted.) However, Koppel[10] has shown that for normal experimental procedures these errors are small compared to the deviations we have noted due to polydispersity. Second, the analysis of the measured values involves some uncertainty due to correlator multiplier overloading, finite channel time, finite number of channels, imperfectly known baseline, and fits made approximately to low order polynomials. In spite of these potential problems, we have demonstrated good agreement between theoretical predictions and the results of a real measurement. This indicates that for at least the mean and variation, the experimental technique is precise enough to extract the true characteristics of polydisperse systems.

Admittedly, real polydisperse systems of interest will not conform in detail to the idealized R distributions investigated in this work. Furthermore, even if they did, the results of a dynamic light scattering measurement will probably not yield enough information. Normally an experiment produces two numbers with reasonable certainty, the mean and width of the D distribution, whereas a real particle distribution probably has more than two degrees of freedom. However, we feel that this investigation is useful to experimenters for two reasons. First, within the context of the ideal model (i.e., Gaussian number distributions of spherical particles), the simulation results specify the consequences of various characteristics of the R distribution upon the measurable quantites. If the number of degrees of freedom may be assumed to be small, then this view of the effects of polydispersity may yield detailed information, again within an ideal context. Second, the simulation procedure may be applied to more interesting distributions, if one has a model for the system. For example, we are at present investigating Boltzmann distributions of micellar aggregates of various shapes.

ACKNOWLEDGMENT

The authors appreciate the helpful comments of Dr. David Cannell during the development of this work.

[1]B. Chu, *Laser Light Scattering* (Academic, New York, 1974).
[2]H. Z. Cummins and E. R. Pike (eds.), *Photon Correlation Spectroscopy and Velocimetry* (Plenum, New York, 1977).
[3]H. Z. Cummins and E. R. Pike (eds.), *Photon Correlation and Light Beating Spectroscopy* (Plenum, New York, 1974).
[4]B. J. Berne and R. Pecora, *Dynamic Light Scattering* (Wiley, New York, 1976).
[5]R. Pecora and Y. Tagami, J. Chem. Phys. **51**, 3298 (1969).
[6]J. E. Frederick *et al.*, Macromolecules **4**, 242 (1971).
[7]H. Z. Cummins *et al.*, Biophys. J. **9**, 518 (1969).
[8]D. S. Thompson, J. Chem. Phys. **54**, 1411 (1971).
[9]C. B. Bargeron, J. Chem. Phys. **61**, 2134 (1974).
[10]D. E. Koppel, J. Chem. Phys. **57**, 4814 (1972).
[11]E. Gulari *et al.*, J. Chem. Phys. **70**, 3965 (1979).
[12]L. Mandel, Prog. Opt. **2**, 181 (1963).
[13]J. Briggs, Phys. Rev. A **18**, 1577 (1978).